ISSN 1674-1056
http://cpb.iphy.ac.cn
http://iopscience.iop.org/cpb
中国物理 B
Chinese Physics
中国物理
Chinese Physics B

Demonstration of superadiabatic population transfer in superconducting qubit

Mengmeng Li(李蒙蒙), Xinsheng Tan(谭新生), Kunzhe Dai(戴坤哲), Peng Zhao(赵鹏), Haifeng Yu(于海峰), Yang Yu(于扬)
Citation: Chin. Phys. B . 2018, 27(6): 063202. **doi:** 10.1088/1674-1056/27/6/063202

Journal homepage: http://cpb.iphy.ac.cn; http://iopscience.iop.org/cpb

What follows is a list of articles you may be interested in

Quantum information processing with nitrogen-vacancy centers in diamond

Gang-Qin Liu(刘刚钦), Xin-Yu Pan(潘新宇)
Chin. Phys. B . 2018, 27(2): 020304. **doi:** 10.1088/1674-1056/27/2/020304

Qubits based on semiconductor quantum dots

Xin Zhang(张鑫), Hai-Ou Li(李海欧), Ke Wang(王柯), Gang Cao(曹刚), Ming Xiao(肖明), Guo-Ping Guo(郭国平)
Chin. Phys. B . 2018, 27(2): 020305. **doi:** 10.1088/1674-1056/27/2/020305

A high-fidelity memory scheme for quantum data buses

Bo-Yang Liu(刘博阳), Wei Cui(崔巍), Hong-Yi Dai(戴宏毅), Xi Chen(陈希), Ming Zhang(张明)
Chin. Phys. B . 2017, 26(9): 090303. **doi:** 10.1088/1674-1056/26/9/090303

Optically pumped quantum M_X–M_R magnetometer with high oscillating magnetic field

Ding Zhi-Chao, Yuan Jie, Wang Zhi-Guo, Yang Kai-Yong, Luo Hui
Chin. Phys. B . 2015, 24(8): 083202. **doi:** 10.1088/1674-1056/24/8/083202

Spectrally selective optical pumping in Doppler-broadened cesium atoms

Zhang Jun-Hai, Zeng Xian-Jin, Li Qing-Meng, Huang Qiang, Sun Wei-Min
Chin. Phys. B . 2013, 22(5): 053202. **doi:** 10.1088/1674-1056/22/5/053202

Demonstration of superadiabatic population transfer in superconducting qubit*

Mengmeng Li(李蒙蒙), Xinsheng Tan(谭新生)†, Kunzhe Dai(戴坤哲), Peng Zhao(赵鹏), Haifeng Yu(于海峰)‡, and Yang Yu(于扬)

National Laboratory of Solid State Microstructures, School of Physics, Nanjing University, Nanjing 210093, *China*

(Received 1 March 2018; revised manuscript received 22 March 2018; published online 10 May 2018)

We implemented the superadiabatic population transfer within the nonadiabatic regime in a two-level superconducting qubit system. To realize the superadiabatic procedure, we added an additional term in the Hamiltonian, introducing an auxiliary counter-diabatic field to cancel the nonadiabatic contribution in the evolution. Based on the superadiabatic procedure, we further demonstrated quantum Phase and NOT gates. These operations, which possess both of the fast and robust features, are promising for quantum information processing.

Keywords: superadiabatic, superconducting qubit, counter-diabatic, fast evolution

PACS: 32.80.Xx, 03.67.Lx, 42.50.Pq **DOI:** 10.1088/1674-1056/27/6/063202

1. Introduction

The adiabatic quantum evolution plays an important role in quantum computation,[1–4] quantum simulation,[5–7] and precision measurements.[8] During an adiabatic evolution, the system follows the instantaneous eigenstate of the Hamiltonian if the system is prepared in an eigenstate at the initial time. It is possible to produce high fidelity population transfer, which is insensitive to the evolution parameters as long as the adiabatic limit is satisfied. Lots of adiabatic techniques have been studied both theoretically and experimentally, such as rapid adiabatic passage (RAP)[9] and stimulated Raman adiabatic passage (STIRAP).[10–13] However, the usual adiabatic transition requires that the process should be sufficiently slow to fulfill the adiabatic limit, which could introduce unwanted errors due to the short decoherence time of the qubits. Therefore, various fast "adiabatic" processes protocols have been proposed to speed up the adiabatic evolutions.[14–18] Among them, the superadiabatic quantum control is believed to be not only remarkably fast but also highly robust against the variations of control parameters. In the superadiabatic protocol, the controlled system follows perfectly the instantaneous adiabatic state of a given Hamiltonian because of the application of an additional control term to cancel the nonadiabatic contribution during a fast evolution.[14–23] Recently superadiabatic protocols have been experimentally realized in the cold atomic ensemble,[24] the NV spin qubit,[25] and the atomic optical lattice system.[26]

In this paper, we demonstrated the superadiabatic population transfer in a superconducting qubit, which is a promising two-level solid-state system for scalable quantum information processing. We found that the superadiabatic population transfers are insensitive to the dynamical evolution times. In our experiment, it is not even necessary to design the exact durations of the controlling fields beforehand. We also realize a quantum NOT gate and a Phase (Z) gate from the superadiabatic population transfer. By comparing the Z gate with that obtained from the generally used Ramsey oscillation, we confirmed the robustness and fast speed of the superadiabatic procedures.

2. Theoretical method

When one microwave field with frequency ω_m and phase φ is applied to a two-level system with energy difference ω_{01} between the states $|0\rangle$ and $|1\rangle$, the Hamiltonian under rotation approximation is given as

$$H_0 = \frac{\hbar}{2}(\Omega_x\sigma_x + \Omega_y\sigma_y + \Delta\sigma_z) = \frac{\hbar}{2}\boldsymbol{B}_0(t)\cdot\boldsymbol{\sigma}, \tag{1}$$

where $\Omega_x = \Omega\cos\varphi$, $\Omega_y = \Omega\sin\varphi$, Ω is the Rabi frequency that results from resonant driving and $\Delta = \omega_{01} - \omega_m$ is the detuning. Since H_0 is the original Hamiltonian used to control the qubit, we can define it as a reference Hamiltonian. $\boldsymbol{B}_0(t)$ is then the effective reference magnetic field expressed in the unit of angular frequency. The instantaneous eigenvectors are

$$|\lambda_+(t)\rangle = \cos\frac{\theta}{2}\mathrm{e}^{-\mathrm{i}\varphi/2}|0\rangle + \sin\frac{\theta}{2}\mathrm{e}^{\mathrm{i}\varphi/2}|1\rangle,$$
$$|\lambda_-(t)\rangle = -\sin\frac{\theta}{2}\mathrm{e}^{-\mathrm{i}\varphi/2}|0\rangle + \cos\frac{\theta}{2}\mathrm{e}^{\mathrm{i}\varphi/2}|1\rangle$$

with the mixing angle $\theta = \arctan[\Omega(t)/\Delta(t)]$. The corresponding eigenvalues are $E_\pm(t) = \pm\hbar\sqrt{\Omega(t)^2 + \Delta(t)^2}/2$.

In the adiabatic approximation, the state driven by $H_0(t)$ is

*Project supported by the National Key Basic Research and Development Program of China (Grant No. 2016YFA0301802) and the National Natural Science Foundation of China (Grant Nos. 11274156, 11504165, 11474152, and 61521001).

†Corresponding author. E-mail: txs.nju@gmail.com

‡Corresponding author. E-mail: hfyu@nju.edu.cn

© 2018 Chinese Physical Society and IOP Publishing Ltd

$$|\Psi_{\pm}(t)\rangle = \exp\left[-\frac{\mathrm{i}}{\hbar}\int_0^t \mathrm{d}t' E_{\pm}(t') - \int_0^t \mathrm{d}t' \langle\lambda_{\pm}(t')|\partial_{t'}\lambda_{\pm}(t')\rangle\right]|\lambda_{\pm}(t)\rangle. \tag{2}$$

Using the reverse engineering approach,[15] one can design a superadiabatic process by controlling the actual evolution Hamiltonian $H_{\mathrm{s}}(t)$. For a superadiabatic Hamiltonian, it is not difficult to find the exact evolving state $|\Psi_{\pm}(t)\rangle$, which satisfies $\mathrm{i}\hbar\partial_t|\Psi_{\pm}(t)\rangle = H_{\mathrm{s}}(t)|\Psi_{\pm}(t)\rangle$. Any time-dependent unitary operator $\widehat{U}(t)$ is the solution of $\mathrm{i}\hbar\partial_t\widehat{U}(t) = H_{\mathrm{s}}(t)\widehat{U}(t)$, where $H_{\mathrm{s}}(t) = \mathrm{i}\hbar(\partial_t\widehat{U}(t))\widehat{U}^{\dagger}(t)$. Therefore, one can find the form of the superadiabatic Hamiltonian to be

$$H_{\mathrm{s}}(t) = \sum_{n=\pm}|\lambda_n(t)\rangle E_n\langle\lambda_n(t)| + \mathrm{i}\hbar\sum_{n=\pm}(\langle\partial_t\lambda_n(t)|\lambda_n(t)\rangle - \langle\lambda_n(t)|\partial_t\lambda_n(t)\rangle\lambda_n(t)|) = H_0(t) + H_1(t). \tag{3}$$

For a spin-1/2 particle, from Eq. (3) one finds that $H_1(t) = \hbar/2\boldsymbol{B}_1(t)\cdot\boldsymbol{\sigma}$ could be the counter-diabatic Hamiltonian that suppresses the nonadiabatic transitions between energy eigenstates and ensures a perfect adiabatic. The counter-diabatic magnetic field is then given by

$$\boldsymbol{B}_1(t) = \frac{\boldsymbol{B}_0(t)\times\dot{\boldsymbol{B}}_0(t)}{|\boldsymbol{B}_0(t)|^2}, \tag{4}$$

which is perpendicular to the reference magnetic field. Due to the high controllability of the superconducting qubit, we may construct different effective magnetic fields to realize the superadiabatic transition. Here we have selected two typical schemes.

2.1. Parameter space in the horizontal plane

For the first scheme, we separate the evolution into four equal time intervals τ. During the total evolution time $T = 4\tau$, the three components of the reference magnetic field $\boldsymbol{B}_0(t) = [\Omega_x, \Omega_y, \Delta]$ are given by

$$\Omega_x(t) = \begin{cases} \Omega_0\left[1-\cos\left(\dfrac{\pi t}{\tau}\right)\right], & 0\leqslant t\leqslant\tau, \\ \Omega_0\left[1+\cos\left(\dfrac{\pi(t-\tau)}{\tau}\right)\right], & \tau < t\leqslant 2\tau, \\ \Omega_0\left[1-\cos\left(\dfrac{\pi(t-2\tau)}{\tau}\right)\right], & 2\tau < t\leqslant 3\tau, \\ \Omega_0\left[1+\cos\left(\dfrac{\pi(t-3\tau)}{\tau}\right)\right], & 3\tau < t\leqslant 4\tau, \end{cases} \tag{5}$$

$$\Omega_y(t) = \begin{cases} \Omega_0\left[\cos\left(\dfrac{\pi t}{\tau}\right)+1\right], & 0\leqslant t\leqslant\tau, \\ \Omega_0\left[\cos\left(\dfrac{\pi(t-\tau)}{\tau}\right)-1\right], & \tau < t\leqslant 2\tau, \\ \Omega_0\left[\cos\left(\dfrac{\pi(t-2\tau)}{\tau}\right)+1\right], & 2\tau < t\leqslant 3\tau, \\ \Omega_0\left[\cos\left(\dfrac{\pi(t-3\tau)}{\tau}\right)-1\right], & 3\tau < t\leqslant 4\tau, \end{cases} \tag{6}$$

$$\Delta(t) = 0, \tag{7}$$

where Ω_0 is a constant Rabi frequency. In Fig. 1(a) we plotted the vector of the reference magnetic field as a function of time. The vector evolves along ABCABC. The evolution path sits in the horizontal plane because $\Delta(t)$ is always zero.

To fulfill the superadiabatic population transfer process, we have to calculate $H_1(t) = \hbar/2\boldsymbol{B}_1(t)\cdot\boldsymbol{\sigma}$ using Eq. (4). The counter-diabatic magnetic field $\boldsymbol{B}_1(t) = [\Omega_{x1}, \Omega_{y1}, \Delta_1]$ is perpendicular to the reference magnetic field and the components are written as

$$\Omega_{x1}(t) = 0, \tag{8}$$

$$\Omega_{y1}(t) = 0, \tag{9}$$

$$\Delta_1(t) = \begin{cases} \dfrac{2\pi\Omega_0^2\sin\left(\dfrac{\pi t}{\tau}\right)}{\tau(\Omega_x^2+\Omega_y^2)}, & 0\leqslant t\leqslant\tau, \\ \dfrac{2\pi\Omega_0^2\sin\left(\dfrac{\pi(t-2\tau)}{\tau}\right)}{\tau(\Omega_x^2+\Omega_y^2)}, & \tau < t\leqslant 2\tau, \\ \dfrac{2\pi\Omega_0^2\sin\left(\dfrac{\pi(t-3\tau)}{\tau}\right)}{\tau(\Omega_x^2+\Omega_y^2)}, & 2\tau < t\leqslant 3\tau, \\ \dfrac{2\pi\Omega_0^2\sin\left(\dfrac{\pi(t-4\tau)}{\tau}\right)}{\tau(\Omega_x^2+\Omega_y^2)}, & 3\tau < t\leqslant 4\tau. \end{cases} \tag{10}$$

For this scheme, during the superadiabatic population transition, the qubit will evolve adiabatically along the latitude of the Bloch sphere if the qubit is initially prepared in the state $(|0\rangle+|1\rangle)/\sqrt{2}$ or $(|0\rangle-|1\rangle)/\sqrt{2}$, both of which are the instantaneous eigenstate of the reference Hamiltonian $H_0(t)$ at $t = 0$.

2.2. Parameter space in the vertical plane

In the second scheme, we also separate the evolution into four equal time intervals τ. During the total evolution time $T = 4\tau$, the components of the reference magnetic field $\boldsymbol{B}_0(t) = [\Omega_x, \Omega_y, \Delta]$ are given by

$$\Omega_x(t) = \begin{cases} \Omega_0\left[\cos\left(\dfrac{\pi t}{\tau}\right)+1\right], & 0\leqslant t\leqslant\tau, \\ \Omega_0\left[\cos\left(\dfrac{\pi(t-\tau)}{\tau}\right)-1\right], & \tau < t\leqslant 2\tau, \\ \Omega_0\left[\cos\left(\dfrac{\pi(t-2\tau)}{\tau}\right)+1\right], & 2\tau < t\leqslant 3\tau, \\ \Omega_0\left[\cos\left(\dfrac{\pi(t-3\tau)}{\tau}\right)-1\right], & 3\tau < t\leqslant 4\tau, \end{cases} \tag{11}$$

$$\Omega_y(t) = 0, \tag{12}$$

$$\Delta(t)=\begin{cases}\Delta_0\left[1-\cos\left(\dfrac{\pi t}{\tau}\right)\right], & 0\leqslant t\leqslant\tau,\\ \Delta_0\left[1+\cos\left(\dfrac{\pi(t-\tau)}{\tau}\right)\right], & \tau<t\leqslant 2\tau,\\ \Delta_0\left[1-\cos\left(\dfrac{\pi(t-2\tau)}{\tau}\right)\right], & 2\tau<t\leqslant 3\tau,\\ \Delta_0\left[1+\cos\left(\dfrac{\pi(t-3\tau)}{\tau}\right)\right], & 3\tau<t\leqslant 4\tau,\end{cases} \tag{13}$$

where Ω_0 is a constant Rabi frequency and Δ_0 is a constant detuning between the qubit driving frequency and the qubit resonance frequency. As shown in Fig. 1(a), the vector of the reference magnetic field evolves along DCEDCE, which is in the vertical plane since $\Omega_y(t)$ is always zero.

Similar to that of the first scheme, we can calculate $H_1(t)=\hbar/2\boldsymbol{B}_1(t)\cdot\boldsymbol{\sigma}$ using Eq. (4). The three components of counter-diabatic magnetic field $\boldsymbol{B}_1(t)=[\Omega_{x1},\Omega_{y1},\Delta_1]$ are

$$\Omega_{x1}(t)=0, \tag{14}$$

$$\Omega_{y1}(t)=\begin{cases}\dfrac{2\pi\Omega_0\Delta_0\sin\left(\dfrac{\pi t}{\tau}\right)}{\tau(\Omega_x^2+\Delta^2)}, & 0\leqslant t\leqslant\tau,\\ \dfrac{2\pi\Omega_0\Delta_0\sin\left(\dfrac{\pi(t-2\tau)}{\tau}\right)}{\tau(\Omega_x^2+\Delta^2)}, & \tau<t\leqslant 2\tau,\\ \dfrac{2\pi\Omega_0\Delta_0\sin\left(\dfrac{\pi(t-3\tau)}{\tau}\right)}{\tau(\Omega_x^2+\Delta^2)}, & 2\tau<t\leqslant 3\tau,\\ \dfrac{2\pi\Omega_0\Delta_0\sin\left(\dfrac{\pi(t-4\tau)}{\tau}\right)}{\tau(\Omega_x^2+\Delta^2)}, & 3\tau<t\leqslant 4\tau,\end{cases} \tag{15}$$

$$\Delta_1(t)=0. \tag{16}$$

For this scheme, the initial state is the instantaneous eigenstate $|0\rangle$ or $|1\rangle$ of the reference Hamiltonian $H_0(t)$ at $t=0$.

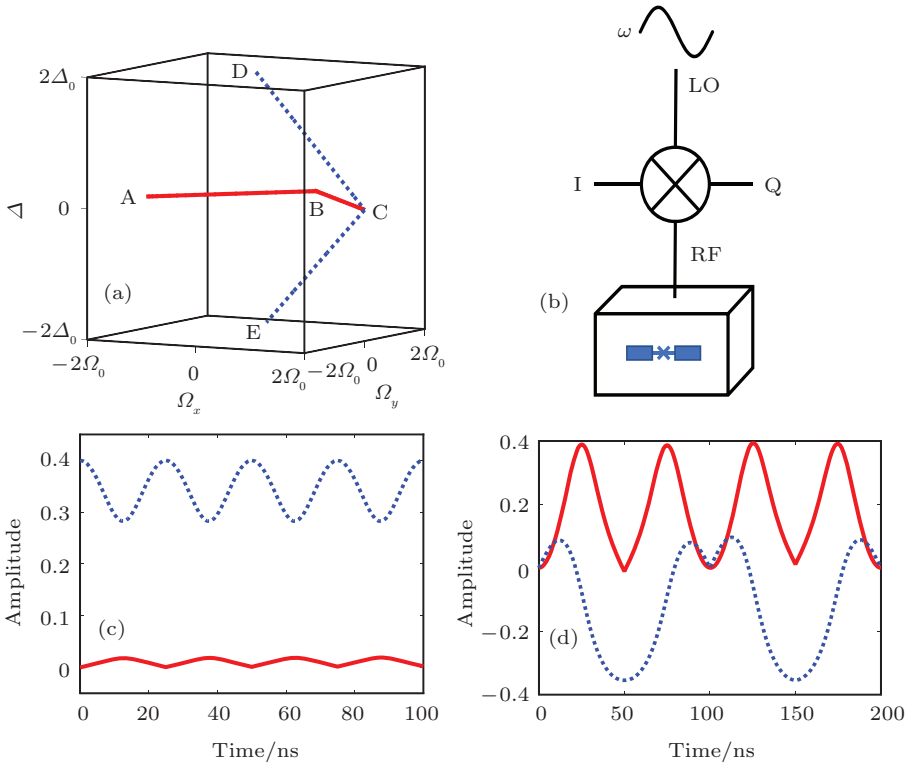


Fig. 1. (color online) (a) Schematic diagram of the reference magnetic field as a function of time. The red line ABC (blue dotted line DCE) represents the evolution path of the vector of the reference magnetic field for the first (second) scheme. (b) Schematic circuit diagram of the qubit control and measurement. The microwave modulated pulses are controlled by the IQ mixer, then they are applied to the 3D cavity input for manipulating the qubit. (c) Examples of the arbitrary waveform signals applied to the I port (the red solid line) and the Q port (the blue dotted line) of the mixer for the first scheme. The output signal from the RF port is the total magnetic field including the reference parts and the counter-diabatic parts. (d) Examples of the arbitrary waveform signals for the second scheme.

3. Experimental setup

The sample used in our experiment is a transmon qubit embedded in a three dimensional aluminium cavity. The main function of the cavity is to control and readout the qubit. Shown in Fig. 1(b) is a schematic diagram of the experimental setup. The sample is cooled in a cryogen-free dilution refrigerator to a base temperature of about 20 mK. In order to measure the qubit, we employed the so-called "high power readout" scheme by using a high-electron-mobility transistor (HEMT) amplifier in the readout line followed by two room-temperature amplifiers. The qubit is manipulated by combining the modulating tones from the Tektronix arbitrary waveform generators (AWG5014c) with a microwave generator via the internal Inphase/Quadrature (I/Q) mixers. For data acquisition, we use the AlazarTech two-channel digitizer (ATS9870) to realize ADCs. From the system calibration experiments, we obtained that the transition frequency between the lowest two energy levels of the transmon is $\omega_{01}=$

$2\pi \times 7.1572$ GHz. The energy relaxation time is $T_1 = 9$ μs and the dephasing time extracted from the Ramsey fringes experiment is $T_\varphi = 6.9$ μs.

In general, realizing the superadiabatic process requires applying the off-resonant microwave with frequency $\omega_{01} - \Delta(t)$. The off-resonant microwave tone may change its frequency during the transfer for a time dependent $\Delta(t)$. In addition, we have to track the qubit state instantaneously in our experiments. We can do this by using another on-resonant microwave to project a qubit toward different axes, completing the qubit state tomography. In order to overcome the difficulty of synchronizing two microwave generators in nanosecond accuracy, we have employed a chirping technique.[27] We chirp the microwave frequency of one microwave generator by controlling the voltages applied on the I/Q mixer. Typical chirped waveforms of the two superadiabatic Hamiltonians applied to the I ports and the Q ports are shown in Figs. 1(c) and 1(d). After we mixed the microwave with the microwave tone of frequency ω_{01} from the LO ports, the final output from the RF ports are microwaves with frequency $\omega_s(t) = \omega - (\Delta(t) + \Delta_1(t))$, amplitude $\Omega_s(t) = \sqrt{\left(\Omega_x(t) + \Omega_{x1}(t)\right)^2 + \left(\Omega_y(t) + \Omega_{y1}(t)\right)^2}$, and phase $\varphi_s(t) = \tan^{-1}\left((\Omega_y(t) + \Omega_{y1}(t))/(\Omega_x(t) + \Omega_{x1}(t))\right)$. Therefore, we can realize the designed effective magnetic fields to do superadiabatic transitions. For a chirping microwave, synchronization is not required when we apply another on-resonant microwave wave pulse. At each step of the evolution, we could extract the qubit state by means of quantum state tomography.[30,31] The z component of the qubit Bloch vector $\langle\sigma_z\rangle$ is determined from the measurement of the ground state population $P_0 = (\langle\sigma_z\rangle + 1)/2$. To measure the x and y components, we apply a resonant $\pi/2$ pulse rotating the qubit about either the x or y axis and then perform the measurement, obtaining $\langle\sigma_y\rangle$ and $\langle\sigma_x\rangle$, respectively.

4. Results and discussion

For the first scheme, we chose $\Omega_0 = 2\pi \times 10$ MHz and the total evolution time $T = 100$ ns. At the beginning, the qubit vector is at $(1,0,0)$ on the Bloch sphere, which is where the position of the instantaneous eigenstate of the reference Hamiltonian is. Then the qubit evolves a cyclic path along the equator, shown in Fig. 2(d). In order to track the system evolution, we measured the qubit in a time interval of 1 ns. In Figs. 2(a), 2(b), and 2(c), we plot the state tomography results of the qubit. It is notable that the accumulated dynamic phase is zero at the end of the sequence. The reason is that the dynamic phases during the first and the second ABC parameter path are opposite hence are canceled out totally. Meanwhile, only a geometric phase γ adds to the initial state and the final qubit state is written as $(|0\rangle e^{-i\gamma/2} + |1\rangle e^{i\gamma/2})/\sqrt{2}$. As a result, this method can be used to measure the Berry phase[28] or realize the superadiabatic geometric quantum gates.[29]

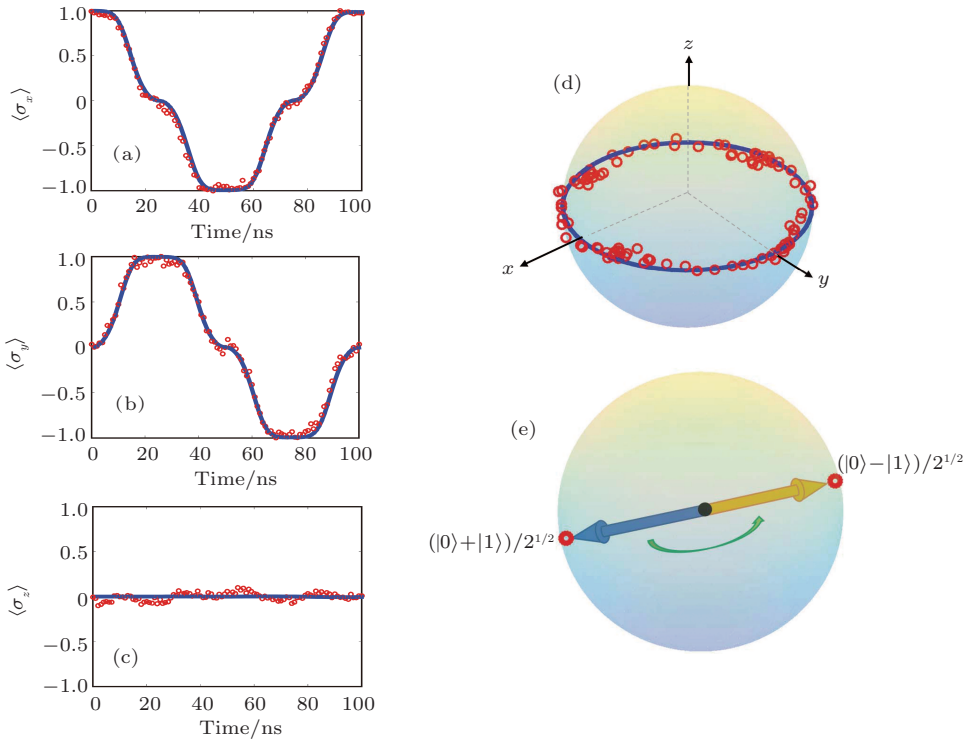


Fig. 2. (color online) State tomography of the qubit for the first scheme. The x component $\langle\sigma_x\rangle$, the y component $\langle\sigma_y\rangle$, and the z component $\langle\sigma_z\rangle$ are plotted in panels (a), (b), and (c), respectively. (d) Trajectory of the qubit state vector on the Bloch sphere. The red circles are experimental data and the associated solid blue lines are the results of the theoretical prediction considering the decoherence and the dephasing. (e) A single qubit Z gate (rotation about the z axis) is realized. The qubit is initially prepared in state $(|0\rangle + |1\rangle)/\sqrt{2}$, and the Z gate is obtained at half of the evolution time.

We now turn to implement the superadiabatic transition with a second scheme. We set $\Omega_0 = \Delta_0 = 2\pi \times 5$ MHz and the total evolution time $T = 200$ ns. As shown in Fig. 3(d), the initial state is at the north pole of the Bloch sphere and the evolution path

of the qubit is along the longitude on the x plane. The state tomography results of the qubit for every 2 ns are shown in Fig. 3(a), 3(b), and 3(c).

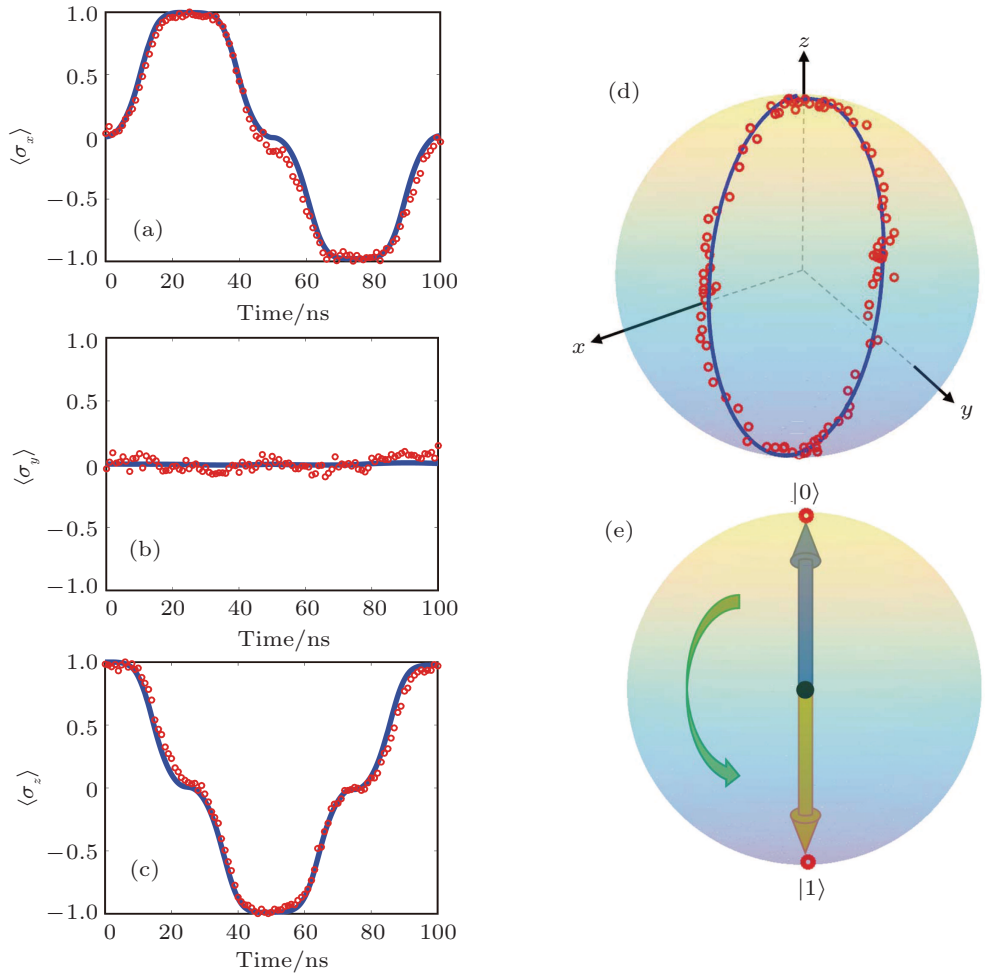


Fig. 3. (color online) State tomography of the qubit for the second scheme. (a) The x projection $\langle\sigma_x\rangle$. (b) The y projection $\langle\sigma_y\rangle$. (c) The z projection $\langle\sigma_z\rangle$. (d) Trajectory of the qubit state vector on the Bloch sphere. The red circles are experimental data and the associated solid blue lines are the results of the theoretical prediction considering the decoherence and the dephasing. (e) A NOT gate is realized so that the initial state $|0\rangle$ becomes $|1\rangle$ at half of the evolution time.

From the evolution of the qubit state vectors on the Bloch spheres in Fig. 2 and Fig. 3, we find that the experimental data and the numerical simulations obtained by solving the master equations agree with each other in general. There are slight deviations which result from the noise of our measurement system and the imperfection of the qubit control and readout. The operation time T is close to the quantum speed limit time $1/\Omega$, therefore we have demonstrated the superadiabatic quantum control within the quantum limit. In order to check the contribution of the counter-diabatic term, we have done experiments with no counter-diabatic control. As shown in Figs. 4(a) and 4(b), for the same evolution time 100 ns and 200 ns the evolution paths deviate completely from the adiabatic trajectory. Actually, our simulation results find that when the evolution times are increased ten times to 1000 ns and 2000 ns, the evolution paths move toward an adiabatic trajectory, which is close to the evolution trajectory of the superadibatic process. Therefore, our superadiabatic control speeds up the adiabatic process more than ten times.

Furthermore, we can compare the fidelity of superadiabatic control with the usual quantum control. From Fig. 2(e) and Fig. 3(e), we obtained that the quantum Z gate and the NOT gate of our superadiabatic evolutions have the fidelities of 99.17% and 98.79%, respectively. On the other hand, we can also realize the quantum Z gate by using the non-linear dependence of the qubit transition frequency on the applied flux. To realize the flux-based Z gate, we first prepare the qubit in the $(|0\rangle + |1\rangle)/\sqrt{2}$ state. Then we change the flux bias, and the qubit will rotate around the z axis due to the change of the eigenenergy. By applying a fast flux bias for a certain time we obtain the quantum Z gate. Shown in Fig. 5 is the gate fidelity as a function of the time deviation from the optimum gate time. The fidelity of the flux bias Z gate exhibits a sharp peak while that of the superadiabatic keeps unchanged for a wide range. This demonstrates that the superadiabatic Z gate is more stable against the time fluctuation than that of the flux-based Z gate.

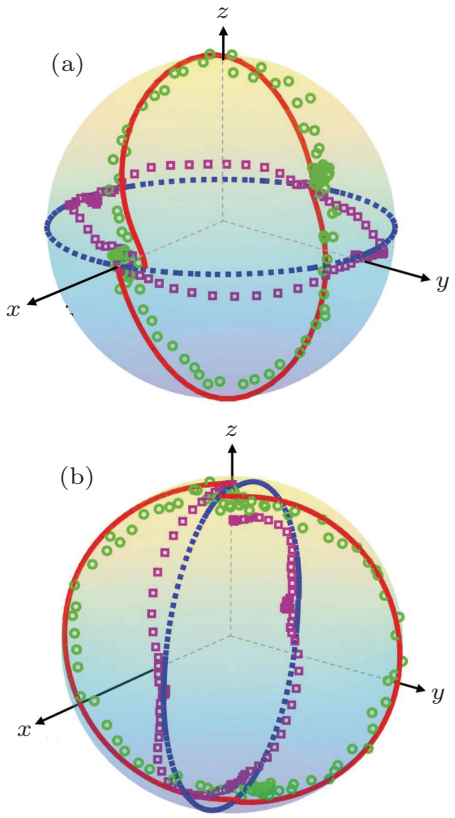


Fig. 4. (color online) Trajectory of the qubit state vector on the Bloch sphere. (a) Evolution trajectory of the qubit in the first scheme with and without the counter-diabatic magnetic field. With no counter-diabatic control, the numerical simulations and experimental results with the evolution time of 100 ns are plotted in the red solid line and the green circles respectively. As a contrast, the blue dotted line is the superadiabatic population transfer path with the same evolution time, and purple squares are simulation results of the adiabatic evolution with the evolution time of 1000 ns. (b) Evolution trajectory of the qubit state vector with and without the counter-diabatic term $H_1(t)$ for the second scheme. With no counter-diabatic control, the red solid line and the green circles are the simulations and experimental results with the evolution time of 200 ns respectively. The superadiabatic process is plotted in the blue dotted line, and the simulation results of the adiabatic evolution with the evolution time of 2000 ns are plotted in purple squares.

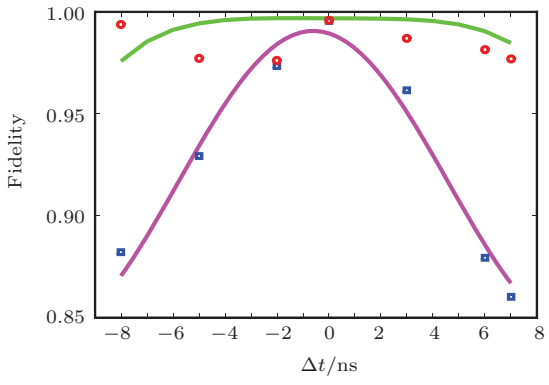


Fig. 5. (color online) The fidelity of the Z gate as a function of the time deviation from the optimum Z gate time. The red circles are the fidelities of the superadiabatic population transfer and the blue squares are the fidelities of the flux-based Z gates.

5. Conclusion

In conclusion, we have demonstrated the superadiabatic population transfer in a two-level superconducting qubit system by applying a counter-diabatic field to ensure a perfect adiabatic evolution. The superadiabatic evolution process has both fast and robust features, which are significant in quantum manipulation.[32] In addition, superadiabatic transition may provide a potential tool for realizing the high-fidelity geometric phase gates.[28,29]

References

[1] Beterov I I, Saffman M, Yakshina E A, Zhukov V P, Tretyakov D B, Entin V M, Ryabtsev I I, Mansell C W, MacCormick C, Bergamini S and Fedoruk M P 2013 *Phys. Rev. A* **88** 010303

[2] Saffman M, Walker T G and Mølmer K 2010 *Rev. Mod. Phys* **82** 2313

[3] Leek P J, Fink J M, Blais A, Bianchetti R, Göppl M, Gambetta J M, Schuster D I, Frunzio L, Schoelkopf R J and Wallraff A 2007 *Science* **318** 5858

[4] Yang Z B, Wu H Z, Zheng S B 2010 *Chin. Phys. B* **19** 094205

[5] Lin Y J, Compton R L, Jiménez-García K, Porto J V and Spielman I B 2009 *Nature* **462** 628

[6] Lin Y J, Jiménez-García K and Spielman I B 2011 *Nature* **471** 83

[7] Dalibard J, Gerbier F, Juzeliūnas G and Öhberg P 2011 *Rev. Mod. Phys* **83** 1523

[8] Kasevich M 2002 *Science* **298** 1363

[9] Kovachy T, Chiow S W and Kasevich M A 2012 *Phys. Rev. A* **86** 011606

[10] Vitanov N V, Halfmann T, Shore B W and Bergmann K 2001 *Ann. Rev. Phys. Chem.* **52** 763

[11] Xu H K, Song C, Liu W Y, Xue G M, Su F F, Deng H, Tian Y, Zheng D N, Han S Y, Zhong Y P, Wang H, Liu Y X and Zhao S P 2016 *Nat. Commun.* **7** 11018

[12] Zhang X Z, Han H L, Han H P, Fan X W 2005 *Chin. Phys* **14** 720

[13] Du Y X, Liang Z T, Huang W, Yan H and Zhu S L 2014 *Phys. Rev. A* **90** 023821

[14] Lim R and Berry M V 1991 *J. Phys. A: Math. Gen.* **24** 3255

[15] Berry M V 2009 *J. Phys. A: Math. Theor.* **42** 365303

[16] Demirplak M and Rice S A 2003 *J. Phys. Chem. A* **107** 9937

[17] Demirplak M and Rice S A 2005 *J. Phys. Chem. B* **109** 6838

[18] Demirplak M and Rice S A 2008 *J. Chem. Phys.* **129** 154111

[19] Torrontegui E, Ibáñez S, Martínez-Garaot S, Modugno M, del Campo A, Guéry-Odelin D, Ruschhaupt A, Chen X, Muga J G 2013 *Adv. At. Mol. Opt. Phys.* **62** 117

[20] Chen X, Lizuain I, Ruschhaupt A, Guefy-Odelin D and Muga J G 2010 *Phys. Rev. Lett.* **105** 123003

[21] Dou F Q, Liu J and Fu L B 2016 *Europhys. Lett.* **116** 60014

[22] Giannelli L and Arimondo E 2014 *Phys. Rev. A* **89** 033419

[23] del Campo A 2013 *Phys. Rev. Lett.* **111** 100502

[24] Du Y X, Liang Z T, Li Y C, Yue X X, Lv Q X, Huang W, Chen X, Yan H and Zhu S L 2016 *Nat. Commun.* **7** 12479

[25] Zhang J F, Shim J H, Niemeyer I, Taniguchi T, Teraji T, Abe H, Onoda S, Yamamoto T, Ohshima T, Isoya J and Suter D 2013 *Phys. Rev. Lett.* **110** 240501

[26] Bason M G, Viteau M, Malossi N, Huillery P, Arimondo E, Ciampini D, Fazio R, Giovannetti V, Mannella R and Morsch O 2012 *Nat. Phys.* **8** 147

[27] Gong M, Zhou Y, Lan D, Fan Y Y, Pan J Z, Yu H F, Chen J, Sun G Z, Yu Y, Han S Y and Wu P H 2016 *Appl. Phys. Lett.* **108** 112602

[28] Zhang Z X, Wang T H, Xiang L, Yao J D, Wu J L and Yin Y 2017 *Phys. Rev. A* **95** 042345

[29] Liang Z T, Yue X X, Lv Q X, Du Y X, Huang W, Yan H and Zhu S L 2016 *Phys. Rev. A* **93** 040305

[30] Liu Y X, Wei L F and Nori F 2004 *Europhys. Lett.* **67** 874

[31] Liu Y X, Wei L F and Nori F 2005 *Phys. Rev. B* **72** 014547

[32] Hollenberg Lloyd C L 2012 *Nat. Phys.* **8** 113